ACS APPLIED NANO MATERIALS

www.acsanm.org

Article

Engineering Conductivity and Performance in Electrorheological Fluids Using a Nanosilica Grafting Approach

Erika Pavlikova, Tomas Plachy,* Michal Urbanek, and Martin Cvek

Cite This: *ACS Appl. Nano Mater.* 2023, 6, 9768−9776

Read Online

ACCESS | Metrics & More | Article Recommendations

ABSTRACT: Carbonization is considered an effective process for the preparation of carbon-rich solids for various applications. Raw carbonaceous particles however often possess high electrical conductivity, limiting their applicability in electrorheology. To address this drawback, the carbonaceous particles prepared from glucose through hydrothermal synthesis, followed by thermal carbonization in an inert atmosphere, were subsequently coated by compact and mesoporous nanosilica, giving rise to semiconducting particles. The successful coating was confirmed using transmission electron microscopy and spectroscopic analysis, and the composite particles were further used as a dispersed phase in electrorheological (ER) fluids of concentration 5 wt %. While an ER fluid based on pure carbonized particles caused a short circuit of the measuring device at the electric field of intensity 1 kV mm^{-1}, the ER behavior of its analogue based on mesoporous silica-coated particles was successfully measured up to 3 kV mm^{-1}, giving a high yield stress exceeding even the values estimated for ER fluids based on similar carbonaceous particles coated with a compact silica layer. Even though the conductivity decreased only about one order of magnitude after the coating process, the dielectric properties of the prepared ER fluid differed significantly, the relaxation process was shifted to lower frequencies, and most importantly, the dielectric relaxation strength increased, indicating an increased amount of interactions. The presence of mesoporous nanosilica further enhanced the sedimentation stability of the ER fluids when compared to its analogue with the compact silica coating, expanding the scope of practical applicability.

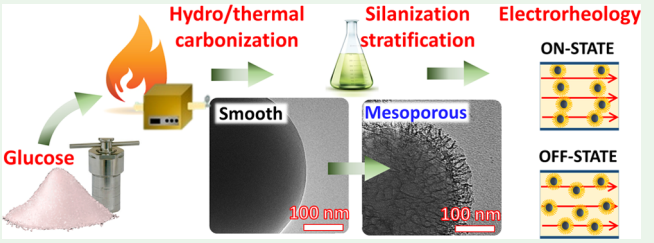

KEYWORDS: *electrorheological fluid, carbonization, electrical conductivity, silica coating, suspension stability*

1. INTRODUCTION

Electrorheological (ER) fluids are systems whose rheological parameters can be controlled via an external electric field. These systems of ER fluids are generally heterogeneous systems composed of a dispersed particulate phase and a nonconducting liquid medium.[1−3] The formation of chain-like structures from the particles within the liquid medium upon the application of an external electric field, called the "ER effect", leads to an abrupt change in the rheological parameters of the system, and the systems then commonly exhibit a certain yield stress, τ_y, that can be defined as a stress that the material can withstand before it starts to flow. This behavior can be utilized in many applications.[4,5]

Nowadays, various carbonaceous particles and their modifications are of high interest for their utilization in many applications, such as capacitors,[6] electromagnetic wave absorption,[7,8] and for conversion of wasted electromagnetic energy into electricity.[9] Carbonaceous particles have also been widely used as a dispersed phase in ER fluids for the last decade owing to their tunable conductivity and ease of preparation.[10,11] Various particulate systems based on carbonized conducting polymers[12−14] or their derivatives[12,15] have been introduced in electrorheology, and their conductivity is commonly controlled through the carbonization temperature.[13] Recently, novel ER fluids based on hydrothermally carbonized green source cellulose exhibiting τ_y > 100 Pa at only 5 wt % of the particles have been introduced.[16] In order to further enhance the ER performance of the ER fluids, composite particles are also of high interest as a dispersed phase in ER fluids because of the possibility to tailor the properties.[17] It is also well known that the optimal conductivity of the particles, to serve as an effective dispersed phase in ER fluids is in the interval 10^{-9}−10^{-5} S cm^{-1} and the particles with higher conductivity, σ, commonly cause a short circuit of a measuring device. In the case of the abovementioned particles,[12,13] when the samples are exposed to carbonization temperatures above 650 °C, the conductivity can exceed ∼10^{-5} S cm^{-1}, and such particles themselves cannot commonly be used in ER fluids.

Received: April 4, 2023
Accepted: May 18, 2023
Published: May 29, 2023

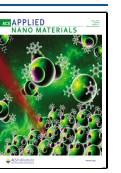

Akhavan et al.[18] prepared core−shell composite particles composed of conducting/nonconducting forms of polyaniline (PANI) coated with lauryl methacrylate. The introduction of a nonconducting shell on PANI in emeraldine hydrochloride resulted in ER fluids with static τ_y exceeding the ER fluid based on uncoated PANI at electric field intensities <3 kV. Moreover, the current drawn significantly decreased for the coated sample, leading to a drop in power consumption, which is further pronounced by controlling the thickness of the shell. Similarly, ER fluids based on PANI nanofibers coated with titania exhibited only slightly lower ER effects when compared to ER fluids based on pure PANI; however, they showed significantly lower leaking currents.[19] Yuan et al.[20] prepared core−shell particles composed of graphene oxide (GO, $\sigma = 3.4 \times 10^{-7}$ S cm^{-1}) or its reduced form (rGO, $\sigma = 6.2$ S cm^{-1}) as the core coated with PANI, yielding final conductivities of 2.5×10^{-9} and 3.6×10^{-9} S cm^{-1}, respectively, for GO/PANI and rGO/PANI. The ER fluid based on GO/PANI exhibited only a slow relaxation process with a relaxation time, t_{rel}, $t_{rel,1} = 1.4 \times 10^{-3}$ s, whereas the one based on the particles with a conducting core from rGO showed a similar relaxation process $t_{rel,1} = 1.3 \times 10^{-3}$ s, arising from the semiconducting PANI shell, as well as fast interfacial polarization with a relaxation of $t_{rel,2} = 1.4 \times 10^{-8}$ s. Therefore, despite similar particle size, morphology, and conductivity, the ER fluid based on rGO/PANI exhibited significantly enhanced ER behavior due to the high conductivity of the core rGO and its enhanced intensity and rate of interfacial polarization.[20] Unlike GO/PANI composites exhibiting a single relaxation process, a system based on poly(ethylaniline)-coated GO exhibited two clear relaxation processes observed at impedance spectroscopy affecting the flow properties of ER fluids.[21] Graphene is another interesting material; however, it is too conducting for its use in electrorheology and is therefore typically modified.[22] The addition of mesoporous silica reduced its conductivity from 5.6 to 2.8×10^{-9} S cm^{-1}, resulting in ER fluids with outstanding ER performance and excellent sedimentation stability.[23] Similarly, the conductivity of two-dimensional (2D) molybdenum sulfide coated with silica[24] or zinc ferrite ($ZnFe_2O_4$) coated with PANI[25] can be reduced, making novel composite particles with moderate conductivity very appealing for ER fluids. Silica can also be used for the preparation of mesoporous or microporous carbonaceous structures with significantly different specific surface areas and ER effects.[11] Nanosilica has been further introduced on the surface of PANI fibers to modify the flow behavior of their ER fluids when compared to pure PANI analogues.[26] Nonconducting surface layers from titania nanocables can be used to modify conducting and nonconducting PANI, and interestingly, ER fluids based on composite particles based on the nonconducting PANI core coated with titania nanocables exhibited more stable flow curves without rupture of the structures due to a change in the polarization rate.[27] In addition, utilization of composite particles can enhance the sedimentation stability of a dispersed phase within a liquid medium.[28]

Preparing composite core−shell particles, where a core is formed of highly conducting particles with a shell from an insulator layer, can thus provide suitable candidates, ER fluids, and interestingly, this approach can lead to outstanding ER effects for ER fluids based on such particles. Furthermore, an insulating layer on the surface of the particles can decrease the current drawn and lower the energy consumption of the measuring device.[18] In the literature, however, particle cores are mainly based on particles whose preparation necessitates toxic chemicals and is tedious, expensive, and complex. This study introduces conducting carbonaceous microspheres prepared from renewable and sustainable source of glucose and their composite with compact and mesoporous silica. While prepared carbonized microspheres exhibited high conductivity for the application in electrorheology, causing a short circuit (and possibly a damage) of a measuring device, their coated analogues had excellent ER effects even at low particle concentration.

2. EXPERIMENTAL SECTION

2.1. Synthesis of a Carbonaceous Precursor. Pure glucose supplied from Sigma-Aldrich (α-D-Glucose, anhydrous, 96%) was first hydrothermally carbonized using a stainless-steel autoclave (total volume 200 mL) when 10 g of glucose was dissolved in 120 mL of demineralized water. The autoclave containing glucose solution was inserted into the heated oven at 180 °C and left for 12 h. After cooling down, hydrothermally carbonized glucose was washed several times with demineralized water, vacuum-filtered, and dried at 60 °C overnight. The second step of carbonization was carried out in a tube furnace (Compact 1600c tube furnace; MTI Corporation) at a high carbonization temperature of 600 °C at a heating rate of 3.3 K min^{-1} where the sample was held at that temperature for 1 h in an argon atmosphere. The sample is labeled as Glu-600.

2.2. Dual-Step Coating Procedure. Glu-600 in the amount of 0.40 g was dispersed in a mixture of 320 mL of ethanol (96%) (EtOH) and 80 mL of demineralized H_2O using the sonication bath (K-12LE, Kraintek, Slovakia). Subsequently, 6 mL of an aqueous ammonia solution (28%) was added under mechanical stirring at 35 °C. The sol−gel process was initiated by injecting 1 mL of TEOS into the system; the reaction was stopped after 6 h. The product, Glu-600 coated with a compact TEOS layer (Glu@SiO_2), was filtered out using the poly(vinylidene fluoride) (PVDF) membrane (pore size of 0.45 μm), washed several times with EtOH, and dried at 50 °C overnight.

In the next step, a mesoporous silica layer (m-SiO_2) was synthesized via a biphase stratification method using Glu@SiO_2 as a core, cetyltrimethylammonium bromide (CTAB) as a template agent, TEOS as a silica source, and triethanolamine (TEA) as a catalyst, as shown recently.[29] In brief, 3.0 g of CTAB and 0.09 g of TEA were dissolved in 30 mL of demineralized H_2O at 60 °C. The 0.25 g of Glu@SiO_2 powder was added and gently mixed for 1 h. The mixture of TEOS/cyclohexane (10 vol %) was carefully injected (0.5 mL min^{-1}) with the help of a programmable syringe pump (AL-220, Aladdin, Switzerland), at low speed (250 rpm) on a magnetic stirrer. After 12 h, the product, Glu@m-SiO_2, was filtered out and washed with EtOH. The surfactant was removed by dispersing Glu@m-SiO_2 in a solution of 80 mg of ammonium nitrate in 120 mL of EtOH; the suspension was heated at 60 °C for 1 h, and the process was repeated three times. The collected Glu@m-SiO_2 was dried at 50 °C overnight. If not stated otherwise, all chemicals were sourced from Sigma-Aldrich.

2.3. Methodology. Field-emission scanning electron microscopy (FE-SEM) was performed on a NanoSEM 450 (FEI Company) using an accelerating voltage of 5 kV (spot size of 2.5). The same device was used for energy-dispersive X-ray (EDX) spectroscopy after employing the Octane Plus detector. Prior to the SEM/EDX, the samples were coated with a thin layer of gold using the sputtering device SC760 (Quorum, UK).

Transmission electron microscopy (TEM) was used to characterize the morphology of the Glu-based samples. TEM images were acquired from a JEM-2100Plus (JEOL, Japan) equipped with a LaB6 emission source at an acceleration voltage of 200 kV. Fourier transform infrared (FTIR) spectroscopy was performed on a Nicolet 6700 (Thermo Scientific) equipped with the ATR accessory and the germanium crystal. The spectra were recorded in the range from 4000 to 700 cm^{-1} at a resolution of 2 cm^{-1} accumulating 64 scans. The

https://doi.org/10.1021/acsanm.3c01475
ACS Appl. Nano Mater. 2023, 6, 9768−9776

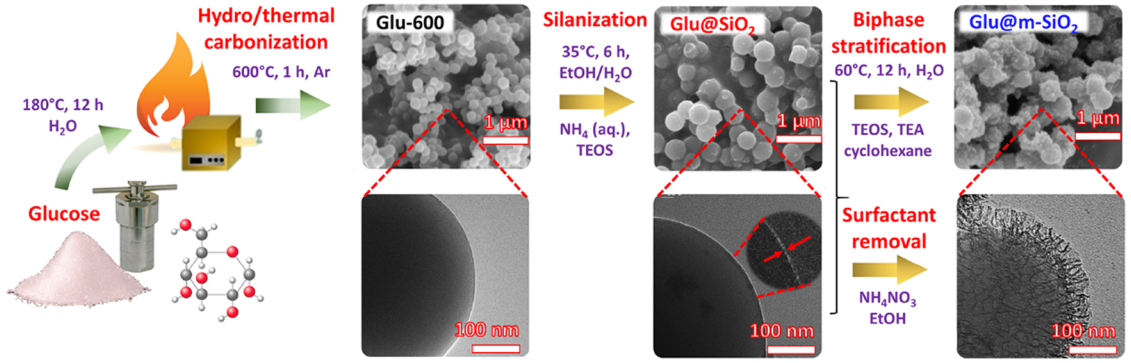

Figure 1. Schematic illustration showing the synthesis protocol of the Glu-600, Glu@SiO_2, and Glu@m-SiO_2 particles with their corresponding FE-SEM and TEM images.

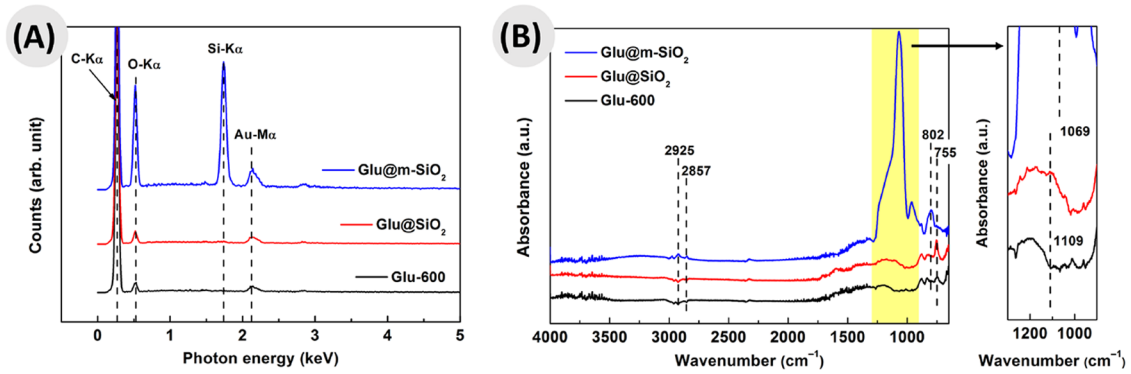

Figure 2. (A) EDX and (B) the FTIR spectra of the Glu-600, Glu@SiO_2, and Glu@m-SiO_2 particles.

conductivity was measured using a two-point method with a Keithley 6517B electrometer (Keithley). The powder was inserted between two gilded brass electrodes and gradually compressed with a defined force at room temperature. The surface area of the prepared powders was estimated using the adsorption/desorption of nitrogen using a Belsorp-mini II analyzer (BEL, Japan) and evaluated by the Brunauer–Emmett–Teller (BET) multipoint method. Impedance spectroscopy was utilized to investigate the dielectric properties of the prepared ER fluids. The measurements were performed in a frequency range of 0.1 Hz–10 MHz utilizing a Concept 50 impedance analyzer (Novocontrol, Germany), equipped with a cylindrical cell. The experimental data were further fitted using a Havriliak–Negami model and an add-in program Solver in Microsoft Excel, applying the least-squares method.

2.4. Electrorheological Characterization. Rheological measurements of prepared ER fluids were performed using a rotational rheometer, the Physica MCR 502 (Anton Paar, Austria), set up with a gap of 0.5 mm between parallel plate geometry (PP25/E/TI) at 25 °C. The fluids were investigated upon an external electric field strength of 0.5–3 kV mm^{-1} as well as without it in a controlled shear rate (CSR) mode at shear rates of 0.01–200 s^{-1}. Prior to each subsequent measurement, the fluid was sheared at a constant 30 s^{-1} to destroy any residual structures and then exposed to the relevant applied electric field for 1 min without shearing to recreate the structures. Leaking current densities were measured using a DC power source (FuG Elektronik, Germany) used for the generation of the electric field.

2.5. Sedimentation Stability. The ER fluids (5 wt %) were thoroughly dispersed using an ultrasonic device (UP400S, Hielscher Technologies, Germany) equipped with a titanium sonotrode (H7) and kept undisturbed in 10 mL vials, under laboratory conditions. Their long-term behavior was monitored on a digital camera, and their sedimentation stability was analyzed via image analysis (ImageJ, National Institute of Health) of the collected records. The sedimentation ratio (H/H_0) was expressed as the height of the particle-rich phase (H) and the total height of the suspension (H_0). Based on the repeated analysis of randomly selected images, the inaccuracy of the reading was estimated to be less than ±0.2%.

3. RESULTS AND DISCUSSION

Unlike the conventional materials for electrorheology that are typically obtained under harsh conditions,[30] herein, glucose was selected as a green precursor accessible from renewable sources to prepare the semiconducting particles (Glu-600) by a facile carbonization technique. To adjust the conductivity of Glu-600 particles, their surface was modified by silanization; the ethoxy groups of TEOS were hydrolyzed into Si–OH and condensed in an alkaline environment on the surface of Glu-600, forming a silane layer (Glu@SiO_2).[31] A subsequent mesoporous structure was included by the surfactant template method. A cationic surfactant, CTAB, formed micelles that acted as a mask for the silica growth.[29] After CTAB removal under basic conditions and washing, radially oriented pores were generated, forming the particles with a mesoporous coating (Glu@m-SiO_2) that improved their properties.

The inspection of our samples began with electron microscopy. While the larger populations of the particles were studied by FE-SEM, the quality of their surface on the individual particles was investigated by TEM. As seen in Figure 1, the neat Glu-600 and Glu@SiO_2 possessed smooth surfaces, uniform sizes, and a spherical shape. In the transmission mode, the latter sample showed a distinct outer contrast difference, which was most likely attributed to a monolayer of SiO_2 (see the inset). The morphology of Glu@m-SiO_2 was greatly changed by mesoporous silica. These particles possessed wrinkled yet uniform structures, which in the transmission

https://doi.org/10.1021/acsanm.3c01475
ACS Appl. Nano Mater. 2023, 6, 9768–9776

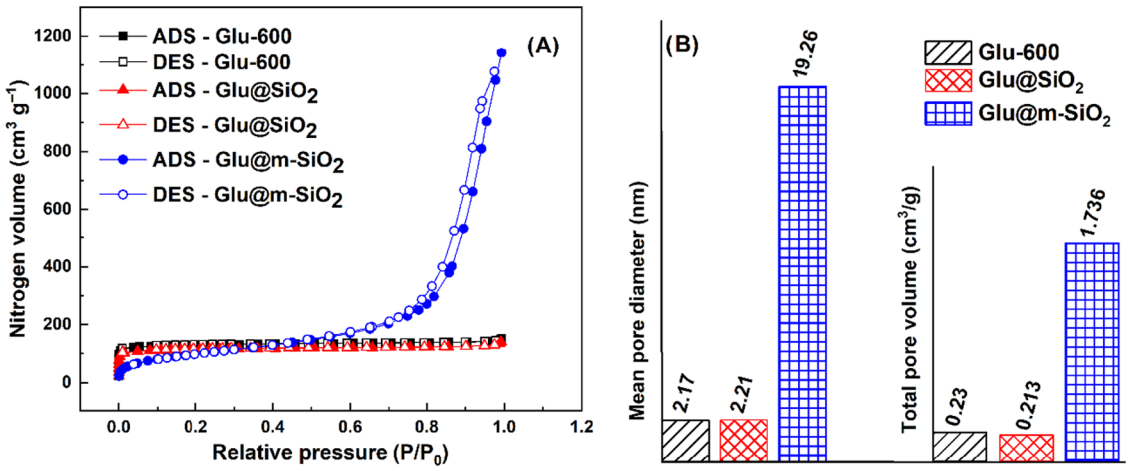

Figure 3. (A) Nitrogen adsorption (ADS)/desorption (DES) isotherms and (B) graphical image of physisorption surface parameters of prepared samples Glu-600, Glu@SiO_2, and Glu@m-SiO_2.

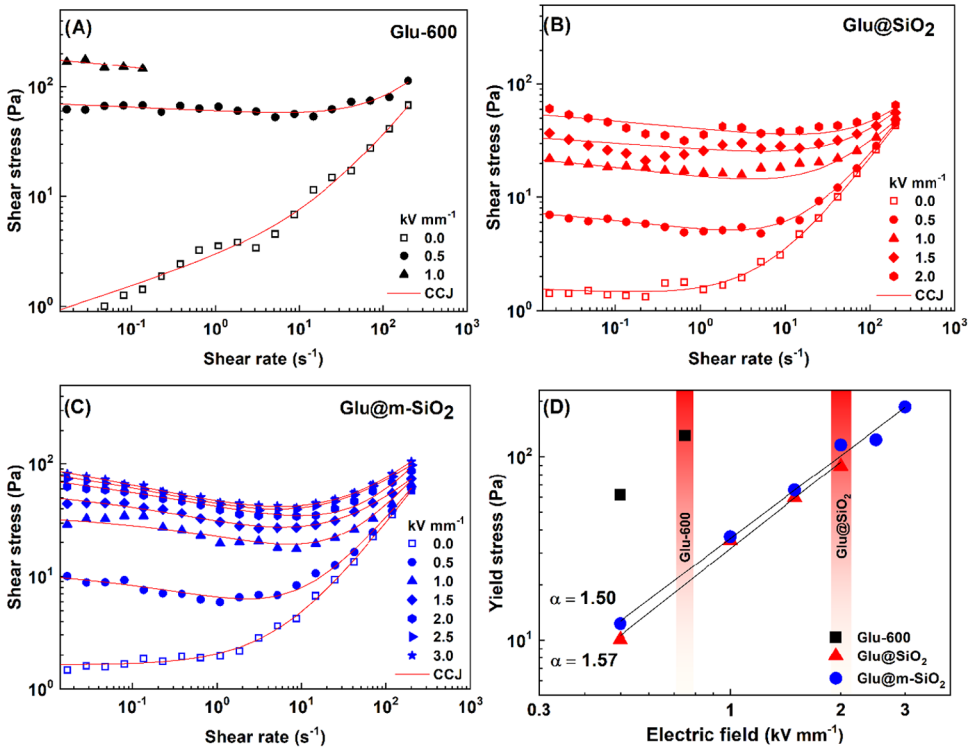

Figure 4. Shear data for the ER fluids containing the Glu-600 (A), Glu@SiO_2 (B), and Glu@m-SiO_2 (C) at the off-state and various electric field strengths. The red solid lines represent the fit of the CCJ model. The dynamic yield stresses (D) as a function of the electric field obtained from the CCJ model. The red bands indicate the critical electric field strengths at which a short circuit occurred for ER fluids based on Glu-600 and Glu@SiO_2.

mode revealed the presence of complex channels, indicating a mesoporous coating.

The differences in chemical composition of the particles' surfaces were investigated using EDX spectroscopy. As observed in Figure 2A, the spectrum of Glu-600 was predominantly composed of carbon (Kα 0.183 eV) with a minor content of oxygen (Kα 0.525 eV), likely as residues from the glucose precursor. The signal for oxygen was higher in the spectrum of Glu@SiO_2, which also showed a subtle peak for silicone (Kα 1.740 eV) coming from the shell. In comparison, the signals for oxygen and silicone were much stronger in the Glu@m-SiO_2, indicating higher concentrations of the coating material. The peak corresponding to gold (Mα 2.123 eV) in all of the samples was related to the conductive sputtered layer.

As a complementary technique, the progress of a dual-step coating was monitored using FTIR spectroscopy. As seen in Figure 2B, the spectrum for Glu-600 was devoid of peaks, which suggests its pure carbonaceous character; the raised levels in the 850−700 cm^{-1} region could be attributed to C−H pendant groups. After coating, the peaks at 2925 (2857) cm^{-1} were assigned to the $-CH_3$ stretching vibration, coming from TEOS. The absorption peaks at 1069 (1109) cm^{-1} were a signature of Si−O−Si stretching, and the peaks at 802 cm^{-1} denoted a coupling of Si−C stretching vibration and $-CH_3$ rocking vibration.[32] While the FTIR spectrum for Glu@SiO_2

https://doi.org/10.1021/acsanm.3c01475
ACS Appl. Nano Mater. 2023, 6, 9768−9776

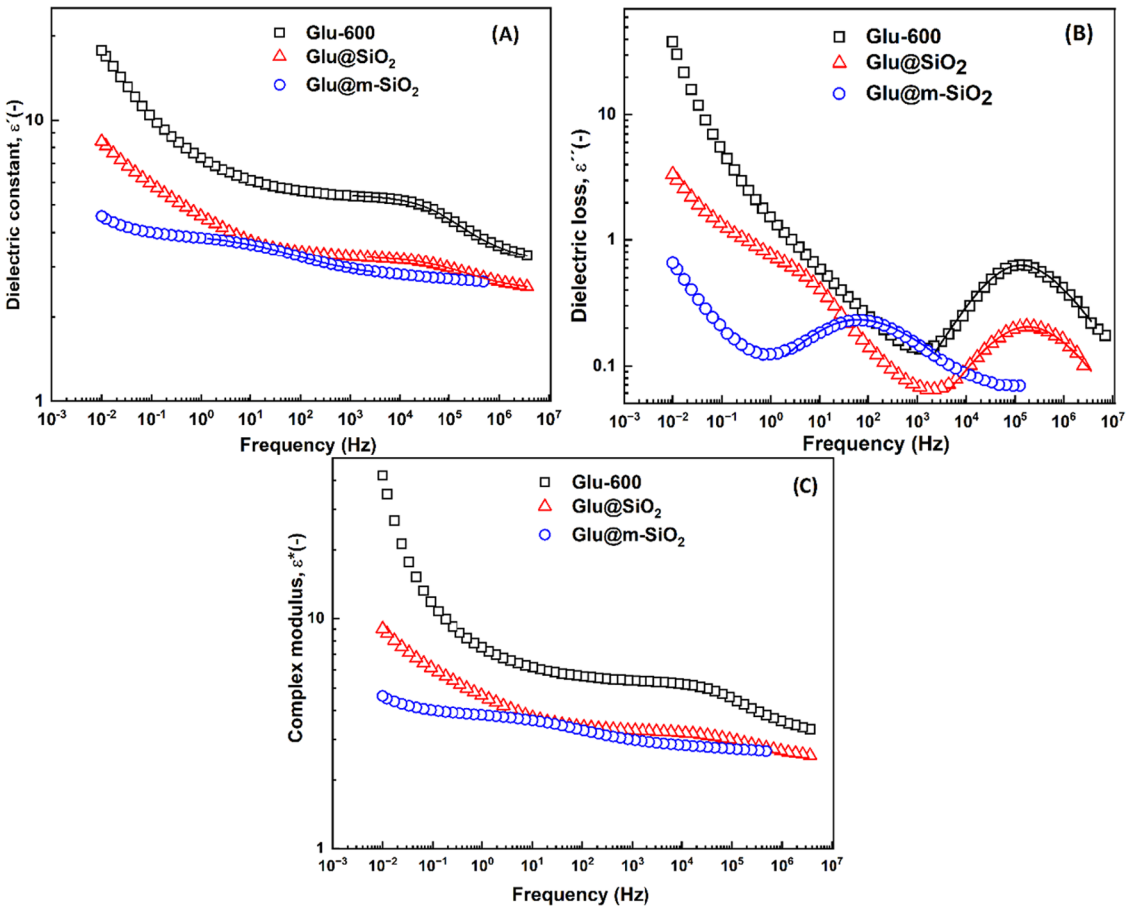

Figure 5. Dependence of real (A) and imaginary (B) parts of complex permittivity and a dependence of the complex modulus (C) on frequency for prepared ER fluids. The solid lines correspond to the fit of the Havriliak−Negami model.

showed subtle differences compared to the reference, possibly indicating the TEOS monolayer, the spectrum for Glu@m-SiO_2 revealed distinct peaks, confirming a thicker layer. It is important to mention that the EDX and FTIR spectra were devoid of peaks related to CTAB,[33] suggesting its effective removal and the high purity of the prepared particles.

The specific surface area of the prepared samples was 4.24 × 10^2, 3.84 × 10^2, and 3.61 × 10^2 m^2/g for particles Glu-600, Glu@SiO_2, and Glu@m-SiO_2, respectively. Because of their high porosity, the specific surface area of the samples did not change significantly after the introduction of mesoporous silica on the surface of the particles. The obtained adsorption curves (Figure 3A) for all prepared samples exhibited a Langmuir-type isotherm with a plateau corresponding to micropore quantity. This value was higher for samples Glu-600 and Glu@SiO_2 when compared to Glu@m-SiO_2 and conventional carbonized materials.[16,34] The adsorption of nitrogen for samples Glu-600 and Glu@SiO_2 took place mainly at low pressures, together with slightly open hysteresis, showing the presence of micropores with a mean pore diameter 2.17 and 2.21 nm, respectively, which is significantly lower than for the sample Glu@m-SiO_2 (19.26 nm), as displayed in Figure 3B. The abrupt increase and hysteresis in the adsorption of nitrogen of the sample Glu@m-SiO_2 indicated the presence of the mesoporous structure that fits well with the coating of the material with mesoporous silica. The total pore volume, representing the total volume of surface pores and very small openings on the particle surface, was found to be the highest for the Glu@m-SiO_2 particles due to the nanosilica coating and its mesoporous character (Figure 1).

The ER investigations of prepared fluids based on Glu-600, Glu@SiO_2, and Glu@m-SiO_2 at a concentration of 5 wt % were performed in the absence and presence of an external electric field. Figure 4 depicts the relationships between shear stress and shear rates for the studied ER fluids in the range of 0−3 kV mm^{-1}. All fluids exhibited slight pseudoplastic behavior in the off-state due to the low concentration of the particles; however, with the application of the electric field, the particles formed chain-like structures, resulting in a certain yield stress, τ_0, defined as a stress at which fluid starts to flow. In the case of Glu-600-based fluid (Figure 4A), high τ_0 of about 62 Pa was already obtained at 0.5 kV mm^{-1} due to the excessively high conductivity of the particles 8.42 × 10^{-6} S cm^{-1}. Therefore, the Glu-600-based fluid was not further measurable at the higher electric field strengths since the leaking currents exceeded the limit of the measuring device. The coating of Glu-600 with a compact SiO_2 layer led to a decrease in conductivity and a slight decrease in the ER effect. The fluid containing Glu@SiO_2 with a conductivity of 3.78 × 10^{-6} S cm^{-1} was measurable in the higher electric fields (Figure 4B); nevertheless, upon reaching 2.5 kV mm^{-1}, a short circuit occurred. In the further step of synthesis, the introduction of a mesoporous silica layer showed the conductivity of Glu@m-SiO_2 as 1.90 × 10^{-7} S cm^{-1}. The fluid prepared based on Glu@m-SiO_2 (Figure 4C) exhibited a

https://doi.org/10.1021/acsanm.3c01475
ACS Appl. Nano Mater. 2023, 6, 9768−9776

higher ER effect when compared to Glu@SiO_2 fluid and measurability even at 3 kV mm^{-1} due to lower leaking currents.

In addition, Figure 4C clearly illustrates that, at low shear rates, shear stresses of Glu@m-SiO_2-based fluid decrease, but from the certain critical shear rate values, it starts to rise since hydrodynamic forces are predominant over electrostatic ones. Flow curves of Glu-600- and Glu@SiO_2-based fluids demonstrated that typical shear stress plateau at low shear rates. For that reason, the ER activity of the fluids was evaluated using the six-parameter Cho−Choi−Jhon (CCJ) model,[35] which properly describes ER behavior[17] at a wide shear rate region and can be read as follows

$$\tau = \frac{\tau_0}{1 + (t_2\dot{\gamma})^{\alpha}} + \eta_{\infty}\left(\frac{1}{1 + (t_3\dot{\gamma})^{\beta}}\right)\dot{\gamma} \quad (1)$$

where τ denotes the shear stress, τ_0 represents the dynamic yield stress, $\dot{\gamma}$ is the shear rate, t_2 and t_3 are time constants, α is the parameter related to the initial decrease in stress, and η_{∞} is the viscosity at high $\dot{\gamma}$, while β can be considered as the corrective term, attaining $0 < \beta \leq 1$. Figure 4A−C shows that the experimental data were fitted with the CCJ model (eq 1) for the fabricated (5 wt %) ER fluids with high accuracy ($R^2 > 0.94$).

As shown in Figure 4D, τ_0 expressing the rigidity of internal structures generated in ER fluids increases with increasing electric field strength (eq 2). The dependence is expressed by the power law model below[36]

$$\tau_0 = q \cdot E^{\alpha} \quad (2)$$

where τ_0 is the dynamic yield stress obtained from the CCJ model, q is the rigidity of the ER system, E is the electric field strength, and α is the slope of a curve fitting the data.

In the case of Glu@SiO_2- and Glu@m-SiO_2-based fluids, the conductivity of the particles is the predominant factor contributing to the ER response; thus, the slope close to 1.5 indicates the conductivity model, while the polarization mechanism is predicted by the slope close to 2. A power law model could not be applied for ER fluid based on Glu-600 since only two yield stress values were available, as can be seen from Figure 4D. However, given the high conductivity of Glu-600 particles, it can be estimated that the yield stresses could also increase with the slope of 1.5.

For high ER effects, ER fluids should generally exhibit strong interfacial polarization between the dispersed phase and a nonconducting liquid medium. All prepared ER fluids exhibited strong interfacial polarization in a desired frequency range approximately belonging to the region where interfacial polarization commonly occurs (Figure 5); moreover, maximum values of the imaginary part of complex permittivity representing the relaxation time exceeded 0.1, representing a strong relaxation process leading to high ER effects.[37] To obtain relevant dielectric parameters, such as t_{rel} and dielectric relaxation strength, $\Delta\varepsilon'$, defined as a difference of a permittivity at static, ε_0', and infinite frequency, ε_{∞}', the measured data were treated using the Havriliak−Negami model (eq 3), where $\varepsilon^*_{(\omega)}$ is a complex permittivity. Parameter ω is the angular frequency, and α and β are shape parameters describing the asymmetry and skewness of the dielectric function, respectively.

$$\varepsilon^*_{(\omega)} = \varepsilon_{\infty}' + \frac{(\varepsilon_0' - \varepsilon_{\infty}')}{(1 + (i\omega \cdot t_{rel})^{\alpha})^{\beta}} \quad (3)$$

While the ER fluid based on Glu-600 and Glu@SiO_2 exhibited short relaxation times 1.5×10^{-6} and 8.9×10^{-7} s, respectively, corresponding to their high conductivity, the ER fluid based on Glu-600 exhibited the highest magnitude of interfacial polarization ($\Delta\varepsilon' = 2.36$) leading to the strongest ER effect among the ER fluids under investigation due to its combination with fast polarization.[27] In composite particles, however, the introduction of smaller particles on the surface can lead to a greater amount of electrostatic interactions,[38] resulting in higher values of $\Delta\varepsilon'$ obtained for ER fluids based on Glu@m-SiO_2 ($\Delta\varepsilon' = 1.21$) when compared with the one based on Glu@SiO_2 ($\Delta\varepsilon' = 0.82$), leading to a higher ER effect. Furthermore, the hopping conductivity mechanism could be applied to describe and clarify the experimental data,[39] where only a single peak of dielectric loss in the case of composite particles was observed. Hopping of the electron between the conducting cores can be partially suppressed, and the process needs much more energy, leading to its decreasing probability, thus lowering the likelihood of this phenomenon due to the insulating layer described by the peak shift to a lower frequency.[39] Thus, even though the relaxation is significantly shifted among the samples, it can be assumed that it represents the relaxation of the carbonaceous core in all of the samples.[39] On the other hand, for all of the samples, the clear conductivity part of the dielectric loss spectra is found at lower frequencies, corresponding to the relatively high conductivity of the particles[40] (Figure 5B). The dependence of complex modulus showed a very similar behavior of samples Glu-600 and Glu@SiO_2 with similar relaxation processes, which were shifted for the sample Glu@m-SiO_2 to lower frequencies (Figure 5C). In this study, all present particles exhibited a high surface area that can lead to an increased amount of electrostatic interactions, explaining such relatively high ER effects of prepared ER fluids with only 5 wt % particle concentration.

The presence of mesoporous nanosilica on the surface of the particles further significantly affected the leaking current density passing through the ER fluids. While ER fluids based on samples Glu-600 and Glu@SiO_2 exhibited short circuits of the instrument at electric field intensities of 1 and 2.5 kV mm^{-1}, respectively, the sample containing Glu@m-SiO_2 with mesoporous nanosilica layers showed very low values of leaking current density (<0.4 μA cm^{-2}) even at the highest electric field intensities (Table 1). Such ER fluid can therefore be considered relatively safe from an application point of view and energy-efficient since it requires only low power consumption.

Table 1. Leaking Current Densities of the Prepared ER Fluids at Various Electric Field Strengths

	leaking current density (μA cm^{-2})		
electric field strength (kV mm^{-1})	Glu-600	Glu@SiO_2	Glu@m-SiO_2
0.5	439.7	25	0.2
1.0	N/A[a]	211	0.3
1.5	N/A[a]	468.3	0.3
2.0	N/A[a]	813.1	0.3
2.5	N/A[a]	N/A[a]	0.3
3.0	N/A[a]	N/A[a]	0.3

[a]Leaking currents were above the limit of the measuring device (i.e., >1000 μA cm^{-2}).

https://doi.org/10.1021/acsanm.3c01475
ACS Appl. Nano Mater. 2023, 6, 9768−9776

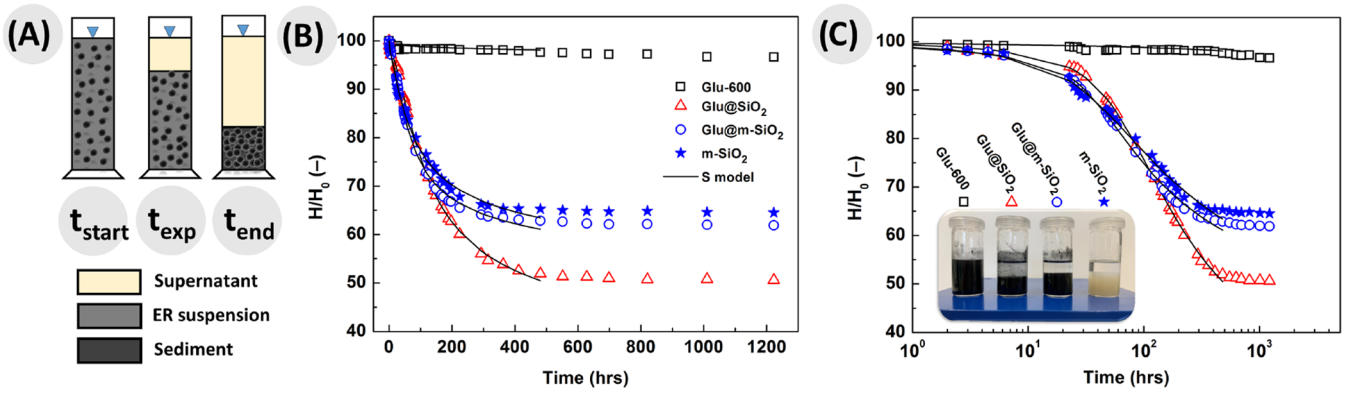

Figure 6. (A) Scheme shows the positions of the interface at the different stages of the sedimentation process. Sedimentation ratio of the ER suspensions containing 5 wt % of Glu-600 (open squares), Glu@SiO_2 (solid circles), Glu@m-SiO_2 (solid diamonds), and m-SiO_2 reference (solid stars) as a function of time in linear (B) and log scale (C); the inset figure shows the ER fluids after ∼50 days of inactivity. The solid lines represent the best fit of the S-model.

The long-term sedimentation stability of four ER fluids was studied simultaneously over the course of ∼50 days. The sedimentation curves were fitted using the "S-model" (eq 4) that was introduced for kaolinite suspensions using the Eulerian−Lagrangian approach[41] and recently validated for bidisperse magnetorheological (MR) suspensions.[42] Unlike a simple exponential decay,[43] the S-model describes the sedimentation curves more effectively by using 5 parameters with a physical meaning. The S-model can be expressed as follows

$$\frac{H(t)}{H_0} = \frac{1}{\left\{\ln\left[\exp(1) + \left(\frac{t}{t_h}\right)^{n_S}\right]\right\}^{m_C}}\left\{1 - \left[\frac{\ln\left(1 + \frac{t}{t_S}\right)}{\ln\left(1 + \frac{10^{45}}{t_C}\right)}\right]\right\} \quad (4)$$

where t represents the experimental time, t_h is related to the induction period of the hindered sedimentation, n_S controls the steepness of the decay representing the maximum settling speed, m_C governs the slope and shape of the curve at the consolidation phase, and t_S and t_C parameters are related to the slope of hindered settling and the final height of the sediment, respectively.

For the investigated ER fluids, the temporal variation of the interface height is sketched in Figure 6A. It is important to mention that the sedimentation behavior of the ER fluids was reflected in the values of the S-model parameters, as summarized in Table 2. As seen in Figure 6B,C, the ER fluid based on Glu-600 exhibited superior kinetic stability without forming a two-phase boundary, i.e., a long flat top (t_h of 115). Thus, it was not possible to optically establish the interface despite observing a minor clarification phenomenon at the later stages of the process.[44] In comparison, Glu@SiO_2 particles were more susceptible to gravitational settling (t_h of 59.5), which was attributed to the presence of silica. Although silica coatings are typically used for counteracting the sedimentation phenomenon (see, e.g., ref 44), in fact, the bulk density of the silica is ∼2.65 g cm^{-3}, while the density of carbonized glucose was reported to be ∼0.6 g cm^{-3} (the value indeed varies with the carbonization temperature),[45] which makes the presence of silica a contributing factor of sedimentation, in this specific case. This phenomenon was projected in a shorter induction period (lower t_h) of the ER fluid based on Glu@SiO_2, compared to the reference. Having this in mind and considering Stoke's law,[46] Glu@m-SiO_2 particles were expected to sediment even faster compared to their compact SiO_2-coated precursors due to a higher total content of silica and a larger particle size, respectively. To investigate the differences, the time in the sedimentation curves was plotted in logarithmic coordinates, intensifying the consolidation phase (Figure 6C). Expectedly, Glu@m-SiO_2 particles exhibited a shorter period of hindered sedimentation; however, their maximum sedimentation rate, n_S, was slightly lower (1.560 vs 1.875), which was attributed to friction effects originating from the mesoporous coating texture (Figure 1). To further prove that the origin of the sedimentation lies in the silica coating, neat m-SiO_2 particles were fabricated (as a control experiment), which showed a comparable sedimentation profile to their Glu@m-SiO_2 variants. Finally, the lack of sedimentation in the ER fluid based on Glu-600 was reflected in a small m_C value (0.077). This parameter yielded higher values (0.267−0.454) for the ER fluids containing the (m-)SiO_2 particles due to the transition into the consolidation phase. The effect of t_S and t_C values was found to be rather insignificant, similarly to what has been observed elsewhere.[41] We note that the consolidation phase was partly excluded from the fitting procedure as the S-model tends to underestimate the experimental data at this zone. However, the differences in the final height of the sediment are clearly distinguishable (Figure 6C, inset), which can be correlated with their capability to be redispersed.[44] The results indicate that addressing the excessive electrical conductivity of Glu-600 was accompanied by a drop in the sedimentation stability due to the SiO_2 coating; however, this phenomenon was mitigated by the application of m-SiO_2, which served as a dual-layer. To conclude, the modified ER fluids were kinetically stable up to 15−20 h, which is a very promising result when compared to the other state-of-the-art ER materials.[47,48]

Table 2. Fitting Parameters of the S-Model for the Investigated ER Fluids

sample ID	t_h	n_S	m_C	t_S	t_C
Glu-600	115	0.25	0.077	34.16	0.101
Glu@SiO_2	59.5	1.875	0.454	1.029	0.001
Glu@m-SiO_2	31.8	1.560	0.311	1.045	0.001
m-SiO_2	31.6	1.569	0.267	0.468	0.001

https://doi.org/10.1021/acsanm.3c01475
ACS Appl. Nano Mater. 2023, 6, 9768−9776

4. CONCLUSIONS

In this study, bio-sourced conducting carbonaceous particles were successfully fabricated by carbonization of glucose, yielding perfect uniform microspheres. These semiconducting particles were coated with compact/mesoporous silica via a biphase stratification method, which slightly suppressed their conductivity from 8.42×10^{-6} to 3.78×10^{-6} S cm^{-1} and 1.90×10^{-7} S cm^{-1}. While ER fluids based on the original particles caused a short circuit of the measuring device even at relatively low electric field intensities, implying a low practical applicability, lowering their conductivity enabled measuring ER performance over the entire tested range of the electric field intensities (0.5−3 kV mm^{-1}). Yield stresses of the prepared ER fluids were estimated utilizing the CCJ model, and interestingly, ER fluids based on mesoporous silica exhibited higher yield stresses than its counterparts based on the intermediate product of the synthesis (i.e., carbonaceous particles with a compact silica layer), despite having about one order of magnitude lower conductivity. Impedance spectroscopy revealed that fluids containing mesoporous silica-coated carbonaceous particles exhibited greater dielectric relaxation due to the presence of mesoporous silica on the particle surfaces, increasing the amount of electrostatic interactions. Although the presence of silica decreased the kinetic stability, the modified ER fluids were stable for 15−20 h. Considering the environmental and technical aspects, such as increased performance with a very low leaking current density and reasonable sedimentation stability, the fabricated ER fluid may find utilization in engineering applications.

AUTHOR INFORMATION

Corresponding Author

Tomas Plachy − *Centre of Polymer Systems, University Institute, Tomas Bata University in Zlin, 760 01 Zlin, Czech Republic;* orcid.org/0000-0002-3806-5307; Email: plachy@utb.cz

Authors

Erika Pavlikova − *Centre of Polymer Systems, University Institute, Tomas Bata University in Zlin, 760 01 Zlin, Czech Republic*

Michal Urbanek − *Centre of Polymer Systems, University Institute, Tomas Bata University in Zlin, 760 01 Zlin, Czech Republic*

Martin Cvek − *Centre of Polymer Systems, University Institute, Tomas Bata University in Zlin, 760 01 Zlin, Czech Republic;* orcid.org/0000-0003-4292-0748

Complete contact information is available at: https://pubs.acs.org/10.1021/acsanm.3c01475

Notes

The authors declare no competing financial interest.

ACKNOWLEDGMENTS

This work was supported by the Ministry of Education, Youth and Sports of the Czech Republic—DKRVO (RP/CPS/2022/003) and DKRVO (RP/CPS/2022/007). M.C. is grateful to J.W. Fulbright Commission in the Czech Republic for the financial support through postdoctoral fellowship (Grant Number: 2022-21-1).

REFERENCES

(1) Li, C. H.; Wang, Z. H.; Wang, L. Y.; Bai, Q.; Wang, B. X.; Hao, C. C. Synthesis and electrorheological properties of TiOF2 @SiO2 cubic-like core/shell nanocomposite. *J. Mol. Liq.* **2022**, *366*, No. 120335.

(2) Zhao, Z. J.; Jin, X.; Liang, Y. R.; Wang, L. M.; Liu, Y. D. TiO_2 nanoparticles dual-modified with ionic liquid and acetic acid for use as electrorheological materials to achieve ultrahigh and stable electro-responsive performances. *ACS Appl. Nano Mater.* **2022**, *5*, 17928−17938.

(3) Kutalkova, E.; Plachy, T. Semi-conducting microspheres formed from glucose for semi-active electric field-responsive electrorheological systems. *Soft Matter* **2022**, *18*, 9037−9044.

(4) Sun, J. F.; Zhang, L. J.; Hui, X. D.; Huang, Y. Z.; Chen, J.; Hu, C. G.; Guo, H. Y.; Qi, S.; Wang, Z. L. Self-powered in-phase sensing and regulating mechanical system enabled by nanogenerator and electrorheological fluid. *Adv. Funct. Mater.* **2023**, *33*, No. 2212248.

(5) Zhao, J. L.; Cao, X. J.; Jing, Y.; Chen, X.; Bai, R. Q.; Yi, J.; Luo, J.; Pu, H. Y. Numerical and experimental study of a novel GER fluid damper based on helical duct flow. *Smart Mater. Struct.* **2022**, *31*, No. 125024.

(6) Chen, X. L.; Shi, T.; Zhong, K. L.; Wu, G. L.; Lu, Y. Capacitive behavior of MoS2 decorated with FeS2@carbon nanospheres. *Chem. Eng. J.* **2020**, *379*, No. 122240.

(7) Zhou, X. F.; Jia, Z. R.; Feng, A. L.; Qu, S. L.; Wang, X. N.; Liu, X. H.; Wang, B. B.; Wu, G. L. Synthesis of porous carbon embedded with NiCo/CoNiO2 hybrids composites for excellent electromagnetic wave absorption performance. *J. Colloid Interface Sci.* **2020**, *575*, 130−139.

(8) Lv, H. L.; Zhou, X. D.; Wu, G. L.; Kara, U. I.; Wang, X. G. Engineering defects in 2D g-C3N4 for wideband, efficient electromagnetic absorption at elevated temperature. *J. Mater. Chem. A* **2021**, *9*, 19710−19718.

(9) Lv, H.; Yao, Y.; Li, S.; Wu, G.; Zhao, B.; Zhou, X.; Dupont, R. L.; Kara, U. I.; Zhou, Y.; Xi, S.; Liu, B.; Che, R.; et al. Staggered circular nanoporous graphene converts electromagnetic waves into electricity. *Nat. Commun.* **2023**, *14*, No. 1982.

(10) Choi, H. J.; Kim, J. W.; Yoon, S. H.; Fujiura, R.; Komatsu, M.; Jhon, M. S. Synthesis and electrorheological characterization of carbonaceous particle suspensions. *J. Mater. Sci. Lett.* **1999**, *18*, 1445−1447.

(11) Qiao, Y. P.; Zhao, X. Electrorheological effect of carbonaceous materials with hierarchical porous structures. *Colloid Surf. A-Physicochem. Eng. Asp.* **2009**, *340*, 33−39.

(12) Plachy, T.; Sedlacik, M.; Pavlinek, V.; Moravkova, Z.; Hajna, M.; Stejskal, J. An effect of carbonization on the electrorheology of poly(p-phenylenediamine). *Carbon* **2013**, *63*, 187−195.

(13) Yin, J. B.; Xia, X. A.; Xiang, L. Q.; Zhao, X. P. Conductivity and polarization of carbonaceous nanotubes derived from polyaniline nanotubes and their electrorheology when dispersed in silicone oil. *Carbon* **2010**, *48*, 2958−2967.

(14) Xia, X. A.; Yin, J. B.; Qiang, P. F.; Zhao, X. P. Electrorheological properties of thermo-oxidative polypyrrole nanofibers. *Polymer* **2011**, *52*, 786−792.

(15) Plachy, T.; Sedlacik, M.; Pavlinek, V.; Stejskal, J.; Graca, M. P.; Costa, L. C. Temperature-dependent electrorheological effect and its description with respect to dielectric spectra. *J. Intell. Mater. Syst. Struct.* **2016**, *27*, 880−886.

(16) Plachy, T.; Kutalkova, E.; Skoda, D.; Holcapkova, P. Transformation of cellulose via two-step carbonizationi to conducting carbonaceous particles and their outstanding electrorheological performance. *Int. J. Mol. Sci.* **2022**, *23*, 5477.

(17) Zhang, B.; Chen, Y.; Zheng, H. N.; Li, C. H.; Ma, L. L.; Zhang, H.; Wang, B. X.; Hao, C. C. Composites of co-doped graphitic C3N4 nanosheets and TiO2 nanoparticles for electrorheological fluid applications. *ACS Appl. Nano Mater.* **2022**, *5*, 1003−1015.

(18) Akhavan, J.; Slack, K.; Wise, V.; Block, H. Coating of polyaniline with an insulating polymer to improve the power

efficiency of electrorheological fluids. *Int. J. Mod. Phys. B* **1999**, *13*, 1931−1939.
(19) Yin, J. B.; Xia, X. A.; Xiang, L. Q.; Zhao, X. P. Coaxial cable-like polyaniline@titania nanofibers: facile synthesis and low power electrorheological fluid application. *J. Mater. Chem.* **2010**, *20*, 7096−7099.
(20) Yuan, J. H.; Wang, Y. D.; Xiang, L. Q.; Zhao, X. P.; Yin, J. B. Understanding the enhanced electrorheological effect of reduced graphene oxide-supported polyaniline dielectric nanoplates by a comparative study with graphene oxide as the support core. *IET Nanodielectr.* **2021**, *4*, 143−154.
(21) Wang, Y.; Yang, M.; Chen, H. G.; Zhao, X. P.; Yin, J. B. Dielectric polarization and electrorheological response of poly-(ethylaniline)-coated reduced graphene oxide nanoflakes with different reduction degrees. *Polymers* **2020**, *12*, No. 2528.
(22) Yin, J. B.; Shui, Y. J.; Chang, R. T.; Zhao, X. P. Graphene-supported carbonaceous dielectric sheets and their electrorheology. *Carbon* **2012**, *50*, 5247−5255.
(23) Yin, J. B.; Chang, R. T.; Kai, Y.; Zhao, X. P. Highly stable and AC electric field-activated electrorheological fluid based on mesoporous silica-coated graphene nanosheets. *Soft Matter* **2013**, *9*, 3910−3914.
(24) Chen, Y.; Sun, W. J.; Zheng, H. N.; Li, C. H.; Zhang, B.; Wang, B. X.; Hao, C. C. Electrorheological response behavior of H2Ti2O5@MoS2@SiO2 core-shell nanoparticles. *Ceram. Int.* **2021**, *47*, 24080−24091.
(25) Kim, H. M.; Kang, S. H.; Choi, H. J. Polyaniline coated ZnFe2O(4) microsphere and its electrorheological and magneto-rheological response. *Colloids Surf., A* **2021**, *626*, No. 127079.
(26) Liu, Y. D.; Fang, F. F.; Choi, H. J. Silica nanoparticle decorated conducting polyaniline fibers and their electrorheology. *Mater. Lett.* **2010**, *64*, 154−156.
(27) Yin, J. B.; Xia, X.; Wang, X. X.; Zhao, X. P. The electrorheological effect and dielectric properties of suspensions containing polyaniline@titania nanocable-like particles. *Soft Matter* **2011**, *7*, 10978−10986.
(28) Zhao, Z. J.; Yin, Y. T.; Jin, X.; Zhang, G. C.; Wang, L. M.; Liu, Y. D.; Choi, H. J. Titanium dioxide nanoparticles modified with disulfonic acid functionalized imidazolium ionic liquids for use as electrorheological materials. *ACS Appl. Nano Mater.* **2021**, *4*, 12382−12392.
(29) Wei, J.; Zou, L. K.; Li, Y. L.; Zhang, X. M. Synthesis of core-shell-structured mesoporous silica nanospheres with dual-pores for biphasic catalysis. *New J. Chem.* **2019**, *43*, 5833−5838.
(30) Mrlik, M.; Cvek, M.; Osicka, J.; Moucka, R.; Sedlacik, M.; Pavlinek, V. Surface-initiated atom transfer radical polymerization from graphene oxide: A way towards fine tuning of electric conductivity and electro-responsive capabilities. *Mater. Lett.* **2018**, *211*, 138−141.
(31) Shao, J. W.; Qiu, J.; Chen, W. F.; Wang, H. F.; Zhang, K. F.; Wu, J.; Yan, L. F. Self-assembled monolayers modified and further silanized graphene nanosheets reinforced silicone rubber with highly mechanical performance. *Compos. Commun.* **2021**, *24*, No. 100666.
(32) Feng, J.; Zhang, Q. L.; Tu, Z. K.; Tu, W. M.; Wan, Z. M.; Pan, M.; Zhang, H. N. Degradation of silicone rubbers with different hardness in various aqueous solutions. *Polym. Degrad. Stab.* **2014**, *109*, 122−128.
(33) Su, G. X.; Yang, C.; Zhu, J. J. Fabrication of gold nanorods with tunable longitudinal surface plasmon resonance peaks by reductive dopamine. *Langmuir* **2015**, *31*, 817−823.
(34) Lee, J.; Choi, Y. C. Pore structure characteristics of foam composite with active carbon. *Materials* **2020**, *13*, No. 4038.
(35) Cho, M. S.; Choi, H. J.; Jhon, M. S. Shear stress analysis of a semiconducting polymer based electrorheological fluid system. *Polymer* **2005**, *46*, 11484−11488.
(36) Seo, Y. P.; Han, S.; Kim, J.; Choi, H. J.; Seo, Y. Analysis of the flow behavior of electrorheological fluids containing polypyrrole nanoparticles or polypyrrole/silica nanocomposite particles. *Rheol. Acta* **2020**, *59*, 415−423.
(37) Hao, T. Electrorheological suspensions. *Adv. Colloid Interface Sci.* **2002**, *97*, 1−35.
(38) Sun, W. J.; Chen, Y.; Zheng, H. N.; Li, C. H.; Zhang, B.; Wang, B. X.; Hao, C. C.; Xing, Z. L. Electrorheological properties of titanium oxide loaded C3N4 composites. *Mater. Chem. Phys.* **2022**, *282*, No. 125941.
(39) Krivka, I.; Prokes, J.; Starykov, O.; Stejskal, J. AC properties of aniline-1,4-phenylenediamine copolymers. *Synth. Met.* **2001**, *119*, 481−482.
(40) Cao, M. S.; Wang, X. X.; Cao, W. Q.; Fang, X. Y.; Wen, B.; Yuan, J. Thermally driven transport and relaxation switching self-powered electromagnetic energy conversion. *Small* **2018**, *14*, No. 1800987.
(41) Kang, X.; Xia, Z.; Wang, J. F.; Yang, W. A novel approach to model the batch sedimentation and estimate the settling velocity, solid volume fraction, and floc size of kaolinite in concentrated solutions. *Colloids Surf., A* **2019**, *579*, No. 123647.
(42) Cvek, M.; Jamatia, T.; Suly, P.; Urbanek, M.; Torres-Mendieta, R. Stable magnetorheological fluids containing bidisperse fillers with compact/mesoporous silica coatings. *Int. J. Mol. Sci.* **2022**, *23*, No. 11044.
(43) Plachy, T.; Cvek, M.; Kozakova, Z.; Sedlacik, M.; Moucka, R. The enhanced MR performance of dimorphic MR suspensions containing either magnetic rods or their non-magnetic analogs. *Smart Mater. Struct.* **2017**, *26*, No. 025026.
(44) Cvek, M.; Mrlik, M.; Moucka, R.; Sedlacik, M. A systematical study of the overall influence of carbon allotrope additives on performance, stability and redispersibility of magnetorheological fluids. *Colloids Surf., A* **2018**, *543*, 83−92.
(45) Myronyuk, I. F.; Mandzyuk, V. I.; Sachko, V. M.; Gun'ko, V. M. Structural features of carbons produced using glucose, lactose, and saccharose. *Nanoscale Res. Lett.* **2016**, *11*, 1−9.
(46) Serrano, L. Z.; Lara, N. O.; Vera, R. R.; Cholico-Gonzalez, D. Removal of Fe(III), Cd(II), and Zn(II) as hydroxides by precipitation-flotation system. *Sustainability* **2021**, *13*, No. 11913.
(47) Ma, N.; Dong, X. F.; Niu, C. G.; Han, B. G. A facile electrostatic spraying method to prepare polyvinylpyrrolidone modified TiO2 particles with improved electrorheological effect. *Soft Mater.* **2017**, *15*, 315−324.
(48) Kovaleva, V. V.; Kuznetsov, N. M.; Istomina, A. P.; Bogdanova, O. I.; Vdovichenko, A. Y.; Streltsov, D. R.; Malakhov, S. N.; Kamyshinsky, R. A.; Chvalun, S. N. Low-filled suspensions of alpha-chitin nanorods for electrorheological applications. *Carbohydr. Polym.* **2022**, *277*, No. 118792.

https://doi.org/10.1021/acsanm.3c01475
ACS Appl. Nano Mater. 2023, 6, 9768−9776